Analysis of $D^+ \to \bar{K}^0 e^+ \nu_e$ and $D^+ \to \pi^0 e^+ \nu_e$ semileptonic decays

M. Ablikim,[1] M. N. Achasov,[9,d] S. Ahmed,[14] X. C. Ai,[1] O. Albayrak,[5] M. Albrecht,[4] D. J. Ambrose,[45] A. Amoroso,[50a,50c] F. F. An,[1] Q. An,[47,38] J. Z. Bai,[1] O. Bakina,[23] R. Baldini Ferroli,[20a] Y. Ban,[31] D. W. Bennett,[19] J. V. Bennett,[5] N. Berger,[22] M. Bertani,[20a] D. Bettoni,[21a] J. M. Bian,[44] F. Bianchi,[50a,50c] E. Boger,[23,b] I. Boyko,[23] R. A. Briere,[5] H. Cai,[52] X. Cai,[1,38] O. Cakir,[41a] A. Calcaterra,[20a] G. F. Cao,[1,42] S. A. Cetin,[41b] J. Chai,[50c] J. F. Chang,[1,38] G. Chelkov,[23,b,c] G. Chen,[1] H. S. Chen,[1,42] J. C. Chen,[1] M. L. Chen,[1,38] S. Chen,[42] S. J. Chen,[29] X. Chen,[1,38] X. R. Chen,[26] Y. B. Chen,[1,38] X. K. Chu,[31] G. Cibinetto,[21a] H. L. Dai,[1,38] J. P. Dai,[34,h] A. Dbeyssi,[14] D. Dedovich,[23] Z. Y. Deng,[1] A. Denig,[22] I. Denysenko,[23] M. Destefanis,[50a,50c] F. De Mori,[50a,50c] Y. Ding,[27] C. Dong,[30] J. Dong,[1,38] L. Y. Dong,[1,42] M. Y. Dong,[1,38,42] Z. L. Dou,[29] S. X. Du,[54] P. F. Duan,[1] J. Z. Fan,[40] J. Fang,[1,38] S. S. Fang,[1,42] X. Fang,[47,38] Y. Fang,[1,*] R. Farinelli,[21a,21b] L. Fava,[50b,50c] F. Feldbauer,[22] G. Felici,[20a] C. Q. Feng,[47,38] E. Fioravanti,[21a] M. Fritsch,[22,14] C. D. Fu,[1] Q. Gao,[1] X. L. Gao,[47,38] Y. Gao,[40] Z. Gao,[47,38] I. Garzia,[21a] K. Goetzen,[10] L. Gong,[30] W. X. Gong,[1,38] W. Gradl,[22] M. Greco,[50a,50c] M. H. Gu,[1,38] Y. T. Gu,[12] Y. H. Guan,[1] A. Q. Guo,[1] L. B. Guo,[28] R. P. Guo,[1] Y. Guo,[1] Y. P. Guo,[22] Z. Haddadi,[25] A. Hafner,[22] S. Han,[52] X. Q. Hao,[15] F. A. Harris,[43] K. L. He,[1,42] F. H. Heinsius,[4] T. Held,[4] Y. K. Heng,[1,38,42] T. Holtmann,[4] Z. L. Hou,[1] C. Hu,[28] H. M. Hu,[1,42] T. Hu,[1,38,42] Y. Hu,[1] G. S. Huang,[47,38] J. S. Huang,[15] X. T. Huang,[33] X. Z. Huang,[29] Z. L. Huang,[27] T. Hussain,[49] W. Ikegami Andersson,[51] Q. Ji,[1] Q. P. Ji,[15] X. B. Ji,[1,42] X. L. Ji,[1,38] L. L. Jiang,[1] L. W. Jiang,[52] X. S. Jiang,[1,38,42] X. Y. Jiang,[30] J. B. Jiao,[33] Z. Jiao,[17] D. P. Jin,[1,38,42] S. Jin,[1,42] T. Johansson,[51] A. Julin,[44] N. Kalantar-Nayestanaki,[25] X. L. Kang,[1] X. S. Kang,[30] M. Kavatsyuk,[25] B. C. Ke,[5] P. Kiese,[22] R. Kliemt,[10] B. Kloss,[22] O. B. Kolcu,[41b,f] B. Kopf,[4] M. Kornicer,[43] A. Kupsc,[51] W. Kühn,[24] J. S. Lange,[24] M. Lara,[19] P. Larin,[14] H. Leithoff,[22] C. Leng,[50c] C. Li,[51] Cheng Li,[47,38] D. M. Li,[54] F. Li,[1,38] F. Y. Li,[31] G. Li,[1] H. B. Li,[1,42] H. J. Li,[1] J. C. Li,[1] Jin Li,[32] K. Li,[13] K. Li,[33] Lei Li,[3] P. R. Li,[42,7] Q. Y. Li,[33] T. Li,[33] W. D. Li,[1,42] W. G. Li,[1] X. L. Li,[33] X. N. Li,[1,38] X. Q. Li,[30] Y. B. Li,[2] Z. B. Li,[39] H. Liang,[47,38] Y. F. Liang,[36] Y. T. Liang,[24] G. R. Liao,[11] D. X. Lin,[14] B. Liu,[34,h] B. J. Liu,[1] C. L. Liu,[5] C. X. Liu,[1] D. Liu,[47,38] F. H. Liu,[35] Fang Liu,[1] Feng Liu,[6] H. B. Liu,[12] H. H. Liu,[1] H. H. Liu,[16] H. M. Liu,[1,42] J. Liu,[1] J. B. Liu,[47,38] J. P. Liu,[52] J. Y. Liu,[1] K. Liu,[40] K. Y. Liu,[27] L. D. Liu,[31] P. L. Liu,[1,38] Q. Liu,[42] S. B. Liu,[47,38] X. Liu,[26] Y. B. Liu,[30] Y. Y. Liu,[30] Z. A. Liu,[1,38,42] Zhiqing Liu,[22] H. Loehner,[25] Y. F. Long,[31] X. C. Lou,[1,38,42] H. J. Lu,[17] J. G. Lu,[1,38] Y. Lu,[1] Y. P. Lu,[1,38] C. L. Luo,[28] M. X. Luo,[53] T. Luo,[43] X. L. Luo,[1,38] X. R. Lyu,[42] F. C. Ma,[27] H. L. Ma,[1] L. L. Ma,[33] M. M. Ma,[1] Q. M. Ma,[1] T. Ma,[1] X. N. Ma,[30] X. Y. Ma,[1,38] Y. M. Ma,[33] F. E. Maas,[14] M. Maggiora,[50a,50c] Q. A. Malik,[49] Y. J. Mao,[31] Z. P. Mao,[1] S. Marcello,[50a,50c] J. G. Messchendorp,[25] G. Mezzadri,[21b] J. Min,[1,38] T. J. Min,[1] R. E. Mitchell,[19] X. H. Mo,[1,38,42] Y. J. Mo,[6] C. Morales Morales,[14] G. Morello,[20a] N. Yu. Muchnoi,[9,d] H. Muramatsu,[44] P. Musiol,[4] Y. Nefedov,[23] F. Nerling,[10] I. B. Nikolaev,[9,d] Z. Ning,[1,38] S. Nisar,[8] S. L. Niu,[1,38] X. Y. Niu,[1] S. L. Olsen,[32] Q. Ouyang,[1,38,42] S. Pacetti,[20b] Y. Pan,[47,38] M. Papenbrock,[51] P. Patteri,[20a] M. Pelizaeus,[4] H. P. Peng,[47,38] K. Peters,[10,g] J. Pettersson,[51] J. L. Ping,[28] R. G. Ping,[1,42] R. Poling,[44] V. Prasad,[1] H. R. Qi,[2] M. Qi,[29] S. Qian,[1,38] C. F. Qiao,[42] L. Q. Qin,[33] N. Qin,[52] X. S. Qin,[1] Z. H. Qin,[1,38] J. F. Qiu,[1] K. H. Rashid,[49,i] C. F. Redmer,[22] M. Ripka,[22] G. Rong,[1,42] Ch. Rosner,[14] X. D. Ruan,[12] A. Sarantsev,[23,e] M. Savrié,[21b] C. Schnier,[4] K. Schoenning,[51] W. Shan,[31] M. Shao,[47,38] C. P. Shen,[2] P. X. Shen,[30] X. Y. Shen,[1,42] H. Y. Sheng,[1] W. M. Song,[1] X. Y. Song,[1] S. Sosio,[50a,50c] S. Spataro,[50a,50c] G. X. Sun,[1] J. F. Sun,[15] S. S. Sun,[1,42] X. H. Sun,[1] Y. J. Sun,[47,38] Y. Z. Sun,[1] Z. J. Sun,[1,38] Z. T. Sun,[19] C. J. Tang,[36] X. Tang,[1] I. Tapan,[41c] E. H. Thorndike,[45] M. Tiemens,[25] I. Uman,[41d] G. S. Varner,[43] B. Wang,[30] B. L. Wang,[42] D. Wang,[31] D. Y. Wang,[31] K. Wang,[1,38] L. L. Wang,[1] L. S. Wang,[1] M. Wang,[33] P. Wang,[1] P. L. Wang,[1] W. Wang,[1,38] W. P. Wang,[47,38] X. F. Wang,[40] Y. Wang,[37] Y. D. Wang,[14] Y. F. Wang,[1,38,42] Y. Q. Wang,[22] Z. Wang,[1,38] Z. G. Wang,[1,38] Z. H. Wang,[47,38] Z. Y. Wang,[1] Z. Y. Wang,[1] T. Weber,[22] D. H. Wei,[11] P. Weidenkaff,[22] S. P. Wen,[1] U. Wiedner,[4] M. Wolke,[51] L. H. Wu,[1] L. J. Wu,[1] Z. Wu,[1,38] L. Xia,[47,38] L. G. Xia,[40] Y. Xia,[18] D. Xiao,[1] H. Xiao,[48] Z. J. Xiao,[28] Y. G. Xie,[1,38] Y. H. Xie,[6] Q. L. Xiu,[1,38] G. F. Xu,[1] J. J. Xu,[1] L. Xu,[1] Q. J. Xu,[13] Q. N. Xu,[42] X. P. Xu,[37] L. Yan,[50a,50c] W. B. Yan,[47,38] W. C. Yan,[47,38] Y. H. Yan,[18] H. J. Yang,[34,h] H. X. Yang,[1] L. Yang,[52] Y. X. Yang,[11] M. Ye,[1,38] M. H. Ye,[7] J. H. Yin,[1] Z. Y. You,[39] B. X. Yu,[1,38,42] C. X. Yu,[30] J. S. Yu,[26] C. Z. Yuan,[1,42] Y. Yuan,[1] A. Yuncu,[41b,a] A. A. Zafar,[49] Y. Zeng,[18] Z. Zeng,[47,38] B. X. Zhang,[1] B. Y. Zhang,[1,38] C. C. Zhang,[1] D. H. Zhang,[1] H. H. Zhang,[39] H. Y. Zhang,[1,38] J. Zhang,[1] J. J. Zhang,[1] J. L. Zhang,[1] J. Q. Zhang,[1] J. W. Zhang,[1,38,42] J. Y. Zhang,[1] J. Z. Zhang,[1,42] K. Zhang,[1] L. Zhang,[1] S. Q. Zhang,[30] X. Y. Zhang,[33] Y. Zhang,[1] Y. Zhang,[1] Y. H. Zhang,[1,38] Y. N. Zhang,[42] Y. T. Zhang,[47,38] Yu Zhang,[42] Z. H. Zhang,[6] Z. P. Zhang,[47] Z. Y. Zhang,[52] G. Zhao,[1] J. W. Zhao,[1,38] J. Y. Zhao,[1] J. Z. Zhao,[1,38] Lei Zhao,[47,38] Ling Zhao,[1] M. G. Zhao,[30] Q. Zhao,[1] Q. W. Zhao,[1] S. J. Zhao,[54] T. C. Zhao,[1] Y. B. Zhao,[1,38] Z. G. Zhao,[47,38] A. Zhemchugov,[23,b] B. Zheng,[48,14] J. P. Zheng,[1,38] W. J. Zheng,[33] Y. H. Zheng,[42] B. Zhong,[28] L. Zhou,[1,38] X. Zhou,[52] X. K. Zhou,[47,38] X. R. Zhou,[47,38] X. Y. Zhou,[1] K. Zhu,[1] K. J. Zhu,[1,38,42] S. Zhu,[1] S. H. Zhu,[46] X. L. Zhu,[40] Y. C. Zhu,[47,38] Y. S. Zhu,[1,42] Z. A. Zhu,[1,42] J. Zhuang,[1,38] L. Zotti,[50a,50c] B. S. Zou,[1] and J. H. Zou[1]

(BESIII Collaboration)

[1]*Institute of High Energy Physics, Beijing 100049, People's Republic of China*
[2]*Beihang University, Beijing 100191, People's Republic of China*
[3]*Beijing Institute of Petrochemical Technology, Beijing 102617, People's Republic of China*
[4]*Bochum Ruhr-University, D-44780 Bochum, Germany*
[5]*Carnegie Mellon University, Pittsburgh, Pennsylvania 15213, USA*
[6]*Central China Normal University, Wuhan 430079, People's Republic of China*
[7]*China Center of Advanced Science and Technology, Beijing 100190, People's Republic of China*
[8]*COMSATS Institute of Information Technology, Lahore, Defence Road,*
Off Raiwind Road, 54000 Lahore, Pakistan
[9]*G.I. Budker Institute of Nuclear Physics SB RAS (BINP), Novosibirsk 630090, Russia*
[10]*GSI Helmholtzcentre for Heavy Ion Research GmbH, D-64291 Darmstadt, Germany*
[11]*Guangxi Normal University, Guilin 541004, People's Republic of China*
[12]*Guangxi University, Nanning 530004, People's Republic of China*
[13]*Hangzhou Normal University, Hangzhou 310036, People's Republic of China*
[14]*Helmholtz Institute Mainz, Johann-Joachim-Becher-Weg 45, D-55099 Mainz, Germany*
[15]*Henan Normal University, Xinxiang 453007, People's Republic of China*
[16]*Henan University of Science and Technology, Luoyang 471003, People's Republic of China*
[17]*Huangshan College, Huangshan 245000, People's Republic of China*
[18]*Hunan University, Changsha 410082, People's Republic of China*
[19]*Indiana University, Bloomington, Indiana 47405, USA*
[20a]*INFN Laboratori Nazionali di Frascati, I-00044 Frascati, Italy*
[20b]*INFN and University of Perugia, I-06100 Perugia, Italy*
[21a]*INFN Sezione di Ferrara, I-44122 Ferrara, Italy*
[21b]*University of Ferrara, I-44122 Ferrara, Italy*
[22]*Johannes Gutenberg University of Mainz, Johann-Joachim-Becher-Weg 45, D-55099 Mainz, Germany*
[23]*Joint Institute for Nuclear Research, 141980 Dubna, Moscow region, Russia*
[24]*Justus-Liebig-Universitaet Giessen, II. Physikalisches Institut,*
Heinrich-Buff-Ring 16, D-35392 Giessen, Germany
[25]*KVI-CART, University of Groningen, NL-9747 AA Groningen, Netherlands*
[26]*Lanzhou University, Lanzhou 730000, People's Republic of China*
[27]*Liaoning University, Shenyang 110036, People's Republic of China*
[28]*Nanjing Normal University, Nanjing 210023, People's Republic of China*
[29]*Nanjing University, Nanjing 210093, People's Republic of China*
[30]*Nankai University, Tianjin 300071, People's Republic of China*
[31]*Peking University, Beijing 100871, People's Republic of China*
[32]*Seoul National University, Seoul 151-747, Korea*
[33]*Shandong University, Jinan 250100, People's Republic of China*
[34]*Shanghai Jiao Tong University, Shanghai 200240, People's Republic of China*
[35]*Shanxi University, Taiyuan 030006, People's Republic of China*
[36]*Sichuan University, Chengdu 610064, People's Republic of China*
[37]*Soochow University, Suzhou 215006, People's Republic of China*
[38]*State Key Laboratory of Particle Detection and Electronics,*
Beijing 100049, Hefei 230026, People's Republic of China
[39]*Sun Yat-Sen University, Guangzhou 510275, People's Republic of China*
[40]*Tsinghua University, Beijing 100084, People's Republic of China*
[41a]*Ankara University, 06100 Tandogan, Ankara, Turkey*
[41b]*Istanbul Bilgi University, 34060 Eyup, Istanbul, Turkey*
[41c]*Uludag University, 16059 Bursa, Turkey*
[41d]*Near East University, Nicosia, North Cyprus, Mersin 10, Turkey*
[42]*University of Chinese Academy of Sciences, Beijing 100049, People's Republic of China*
[43]*University of Hawaii, Honolulu, Hawaii 96822, USA*
[44]*University of Minnesota, Minneapolis, Minnesota 55455, USA*
[45]*University of Rochester, Rochester, New York 14627, USA*
[46]*University of Science and Technology Liaoning, Anshan 114051, People's Republic of China*
[47]*University of Science and Technology of China, Hefei 230026, People's Republic of China*
[48]*University of South China, Hengyang 421001, People's Republic of China*
[49]*University of the Punjab, Lahore-54590, Pakistan*
[50a]*University of Turin, I-10125 Turin, Italy*
[50b]*University of Eastern Piedmont, I-15121 Alessandria, Italy*
[50c]*INFN, I-10125 Turin, Italy*

[51]Uppsala University, Box 516, SE-75120 Uppsala, Sweden
[52]Wuhan University, Wuhan 430072, People's Republic of China
[53]Zhejiang University, Hangzhou 310027, People's Republic of China
[54]Zhengzhou University, Zhengzhou 450001, People's Republic of China

Using 2.93 fb^{-1} of data taken at 3.773 GeV with the BESIII detector operated at the BEPCII collider, we study the semileptonic decays $D^+ \to \bar{K}^0 e^+ \nu_e$ and $D^+ \to \pi^0 e^+ \nu_e$. We measure the absolute decay branching fractions $\mathcal{B}(D^+ \to \bar{K}^0 e^+ \nu_e) = (8.60 \pm 0.06 \pm 0.15) \times 10^{-2}$ and $\mathcal{B}(D^+ \to \pi^0 e^+ \nu_e) = (3.63 \pm 0.08 \pm 0.05) \times 10^{-3}$, where the first uncertainties are statistical and the second systematic. We also measure the differential decay rates and study the form factors of these two decays. With the values of $|V_{cs}|$ and $|V_{cd}|$ from Particle Data Group fits assuming Cabibbo-Kobayashi-Maskawa (CKM) unitarity, we obtain the values of the form factors at $q^2 = 0$, $f_+^K(0) = 0.725 \pm 0.004 \pm 0.012$, and $f_+^\pi(0) = 0.622 \pm 0.012 \pm 0.003$. Taking input from recent lattice QCD calculations of these form factors, we determine values of the CKM matrix elements $|V_{cs}| = 0.944 \pm 0.005 \pm 0.015 \pm 0.024$ and $|V_{cd}| = 0.210 \pm 0.004 \pm 0.001 \pm 0.009$, where the third uncertainties are theoretical.

I. INTRODUCTION

In the Standard Model (SM) of particle physics, the mixing between the quark flavors in the weak interaction is parametrized by the Cabibbo-Kobayashi-Maskawa (CKM) matrix, which is a 3×3 unitary matrix. Since the CKM matrix elements are fundamental parameters of the SM, precise determinations of these elements are very important for tests of the SM and searches for new physics beyond the SM.

Since the effects of strong and weak interactions can be well separated in semileptonic D decays, these decays are excellent processes from which we can determine the magnitude of the CKM matrix element $V_{cs(d)}$. In the SM, neglecting the lepton mass, the differential decay rate for $D^+ \to P e^+ \nu_e$ ($P = \bar{K}^0$ or π^0) is given by [1]

$$\frac{d\Gamma}{dq^2} = X \frac{G_F^2}{24\pi^3} |V_{cs(d)}|^2 p^3 |f_+(q^2)|^2, \qquad (1)$$

*Corresponding author.
fangy@ihep.ac.cn
[a]Also at Bogazici University, 34342 Istanbul, Turkey.
[b]Also at Moscow Institute of Physics and Technology, Moscow 141700, Russia.
[c]Also at Functional Electronics Laboratory, Tomsk State University, Tomsk, 634050, Russia.
[d]Also at Novosibirsk State University, Novosibirsk, 630090, Russia.
[e]Also at NRC "Kurchatov Institute," PNPI, 188300, Gatchina, Russia.
[f]Also at Istanbul Arel University, 34295 Istanbul, Turkey.
[g]Also at Goethe University Frankfurt, 60323 Frankfurt am Main, Germany.
[h]Also at Key Laboratory for Particle Physics, Astrophysics and Cosmology, Ministry of Education; Shanghai Key Laboratory for Particle Physics and Cosmology; Institute of Nuclear and Particle Physics, Shanghai 200240, People's Republic of China.
[i]Government College Women University, Sialkot—51310, Punjab, Pakistan.

where G_F is the Fermi constant, $V_{cs(d)}$ is the corresponding CKM matrix element, p is the momentum of the meson P in the rest frame of the D meson, q^2 is the squared 4-momentum transfer, i.e., the invariant mass of the lepton and neutrino system, and $f_+(q^2)$ is the form factor which parametrizes the effect of the strong interaction. In Eq. (1), X is a multiplicative factor due to isospin, which equals 1 for the decay $D^+ \to \bar{K}^0 e^+ \nu_e$ and $1/2$ for the decay $D^+ \to \pi^0 e^+ \nu_e$.

In this article, we report the experimental study of $D^+ \to \bar{K}^0 e^+ \nu_e$ and $D^+ \to \pi^0 e^+ \nu_e$ decays using a 2.93 fb^{-1} [2] data set collected at a center-of-mass energy of $\sqrt{s} = 3.773$ GeV with the BESIII detector operated at the BEPCII collider. Throughout this paper, the inclusion of charge conjugate channels is implied.

The paper is structured as follows. We briefly describe the BESIII detector and the Monte Carlo (MC) simulation in Sec. II. The event selection is presented in Sec. III. The measurements of the absolute branching fractions and the differential decay rates are described in Secs. IV and V, respectively. In Sec. VI we discuss the determination of form factors from the measurements of decay rates, and finally, in Sec. VII, we present the determination of the magnitudes of the CKM matrix elements V_{cs} and V_{cd}. A brief summary is given in Sec. VIII.

II. BESIII DETECTOR

The BESIII detector is a cylindrical detector with a solid-angle coverage of 93% of 4π, designed for the study of hadron spectroscopy and τ-charm physics. The BESIII detector is described in detail in Ref. [3]. Detector components particularly relevant for this work are (1) the main drift chamber (MDC) with 43 layers surrounding the beam pipe, which performs precise determination of charged particle trajectories and provides a measurement of the

TABLE I.   The ΔE requirements, the M_{BC} signal regions, the yields of the D^- tags (N_{tag}) reconstructed in data, and the reconstruction efficiency (ε_{tag}) of D^- tags. The uncertainties are statistical only.

Tag mode	ΔE (MeV)	M_{BC} (GeeV/c^2)	N_{tag}	ε_{tag} (%)
$D^- \to K^+\pi^-\pi^-$	$(-45, 45)$	$(1.8640, 1.8770)$	806830 ± 1070	51.8 ± 0.1
$D^- \to K^0_S\pi^-$	$(-45, 45)$	$(1.8640, 1.8770)$	102755 ± 372	56.2 ± 0.2
$D^- \to K^0_S K^-$	$(-45, 45)$	$(1.8650, 1.8770)$	19566 ± 185	52.1 ± 0.5
$D^- \to K^+ K^- \pi^-$	$(-50, 50)$	$(1.8650, 1.8780)$	68216 ± 966	41.2 ± 0.3
$D^- \to K^+\pi^-\pi^-\pi^0$	$(-78, 78)$	$(1.8620, 1.8790)$	271571 ± 2367	27.3 ± 0.1
$D^- \to \pi^+\pi^-\pi^-$	$(-45, 45)$	$(1.8640, 1.8770)$	32150 ± 371	56.9 ± 0.7
$D^- \to K^0_S\pi^-\pi^0$	$(-75, 75)$	$(1.8640, 1.8790)$	245303 ± 1273	31.3 ± 0.1
$D^- \to K^+\pi^-\pi^-\pi^-\pi^+$	$(-52, 52)$	$(1.8630, 1.8775)$	30923 ± 733	22.1 ± 0.2
$D^- \to K^0_S\pi^-\pi^-\pi^+$	$(-50, 50)$	$(1.8640, 1.8770)$	125740 ± 1203	33.0 ± 0.2
Sum			1703054 ± 3405	

specific ionization energy loss (dE/dx), (2) a time-of-flight system (TOF) made of plastic scintillator counters, which are located outside of the MDC and provide additional charged particle identification information, and (3) the electromagnetic calorimeter (EMC) consisting of 6240 CsI(Tl) crystals used to measure the energy of photons and to identify electrons.

A GEANT4-based [4] MC simulation software [5], which contains the detector geometry description and the detector response, is used to optimize the event selection criteria, study possible backgrounds, and determine the reconstruction efficiencies. The production of the $\psi(3770)$, initial state radiation production of $\psi(3686)$ and J/ψ, as well as the continuum processes of $e^+e^- \to \tau^+\tau^-$ and $e^+e^- \to q\bar{q}$ ($q = u, d, s$) are simulated by the MC event generator KKMC [6]; the known decay modes are generated by EVTGEN [7] with the branching fractions set to the world average values from the Particle Data Group (PDG) [8], while the remaining unknown decay modes are modeled by LUNDCHARM [9]. We also generate signal MC events consisting of $\psi(3770) \to D^+D^-$ events in which the D^- meson decays to all possible final states, and the D^+ meson decays to a hadronic or a semileptonic decay final state being investigated. In the generation of signal MC events, the semileptonic decays $D^+ \to \bar{K}^0 e^+\nu_e$ and $D^+ \to \pi^0 e^+\nu_e$ are modeled by the modified pole parametrization (see Sec. VI A).

III. EVENT RECONSTRUCTION

The center-of-mass energy of 3.773 GeV corresponds to the peak of the $\psi(3770)$ resonance, which decays predominantly into $D\bar{D}$ ($D^0\bar{D}^0$ or D^+D^-) meson pairs. In events where a D^- meson is fully reconstructed, the remaining particles must all be decay products of the accompanying D^+ meson. In the following, the reconstructed meson is called "tagged D^-" or "D^- tag." In a tagged D^- data sample, the recoiling D^+ decays to $\bar{K}^0 e^+\nu_e$ or $\pi^0 e^+\nu_e$ can be cleanly isolated and used to measure the branching fraction and differential decay rates.

A. Selection of D^- tags

We reconstruct D^- tags in the following nine hadronic modes: $D^- \to K^+\pi^-\pi^-$, $D^- \to K^0_S\pi^-$, $D^- \to K^0_S K^-$, $D^- \to K^+K^-\pi^-$, $D^- \to K^+\pi^-\pi^-\pi^0$, $D^- \to \pi^+\pi^-\pi^-$,[1] $D^- \to K^0_S\pi^-\pi^0$, $D^- \to K^+\pi^-\pi^-\pi^-\pi^+$, and $D^- \to K^0_S\pi^-\pi^-\pi^+$. The selection criteria of D^- tags used here are the same as those described in Ref. [10]. Tagged D^- mesons are identified by their beam-energy-constrained mass $M_{BC} \equiv \sqrt{E^2_{beam}/c^4 - |\vec{p}_{tag}|^2/c^2}$, where E_{beam} is the beam energy, and $\vec{p}_{tag}$ is the measured 3-momentum of the tag candidate.[2] We also use the variable $\Delta E \equiv E_{tag} - E_{beam}$, where E_{tag} is the measured energy of the tag candidate, to select the D^- tags. Each tag candidate is subjected to a tag mode-dependent ΔE requirement as shown in Table I. If there are multiple candidates per tag mode for an event, the one with the smallest value of $|\Delta E|$ is retained.

The M_{BC} distributions for the nine D^- tag modes are shown in Fig. 1. A binned extended maximum likelihood fit is used to determine the number of tagged D^- events for each of the nine modes. We use the MC simulated signal shape convolved with a double-Gaussian resolution function to represent the beam-energy-constrained mass signal for the D^- daughter particles, and an ARGUS function [11] multiplied by a third-order polynomial [12,13] to describe the background shape for the M_{BC} distributions. In the fits all parameters of the double-Gaussian function, the ARGUS function, and the polynomial function are left free. The solid lines in Fig. 1 show the best fits, while the dashed lines show the fitted background shapes. The numbers of the D^- tags (N_{tag}) within the M_{BC} signal regions given by the two vertical lines in Fig. 1 are summarized in Table I. In total, we find 1703054 ± 3405 single D^- tags reconstructed in data. The

---

[1]We veto the $K^0_S\pi^-$ candidates when a $\pi^+\pi^-$ invariant mass falls within the K^0_S mass window.

[2]In this analysis, all 4-momentum vectors measured in the laboratory frame are boosted to the e^+e^- center-of-mass frame.
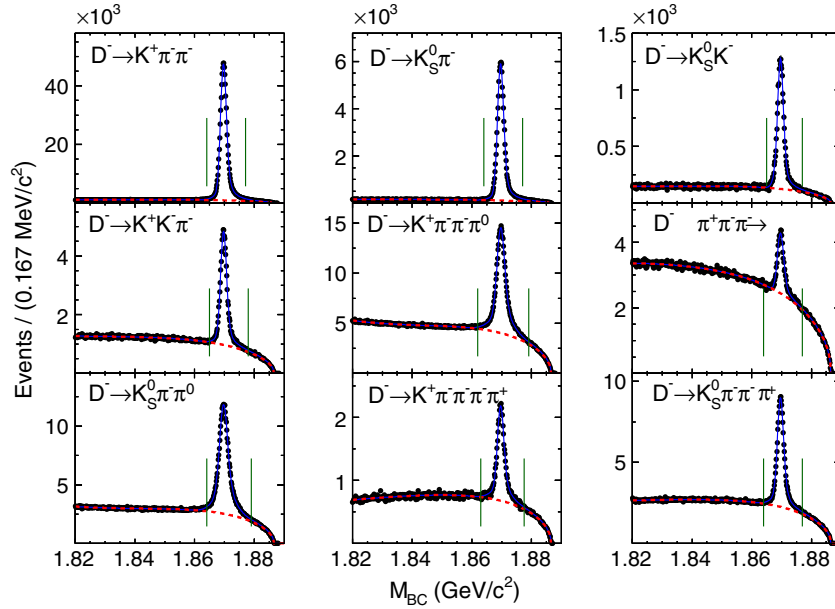
FIG. 1. Fits (solid lines) to the M_{BC} distributions (points with error bars) in data for nine D^- tag modes. The two vertical lines show the tagged D^- mass regions.

reconstruction efficiencies of the single D^- tags, ϵ_{tag}, as determined with the MC simulation, are shown in Table I.

B. Reconstruction of semileptonic decays

Candidates for semileptonic decays are selected from the remaining tracks in the system recoiling against the D^- tags. The dE/dx, TOF, and EMC measurements (deposited energy and shape of the electromagnetic shower) are combined to form confidence levels for the e hypothesis (CL_e), the π hypothesis (CL_π), and the K hypothesis (CL_K). Positron candidates are required to have CL_e greater than 0.1% and to satisfy $CL_e/(CL_e + CL_\pi + CL_K) > 0.8$. In addition, we include the 4-momenta of nearby photons within 5° of the direction of the positron momentum to partially account for final-state-radiation energy losses (FSR recovery). The neutral kaon candidates are built from pairs of oppositely charged tracks that are assumed to be pions. For each pair of charged tracks, a vertex fit is performed and the resulting track parameters are used to calculate the invariant mass, $M(\pi^+\pi^-)$. If $M(\pi^+\pi^-)$ is in the range $(0.484, 0.512)$ GeeV/c^2, the $\pi^+\pi^-$ pair is treated as a K_S^0 candidate and is used for further analysis. The neutral pion candidates are reconstructed via the $\pi^0 \to \gamma\gamma$ decays. For the photon selection, we require the energy of the shower deposited in the barrel (end-cap) EMC greater than 25 (50) MeV and the shower time be within 700 ns of the event start time. In addition, the angle between the photon and the nearest charged track is required to be greater than 10°. We accept the pair of photons as a π^0 candidate if the invariant mass of the two photons $M(\gamma\gamma)$ is in the range $(0.110, 0.150)$ GeV/c^2.

A 1-constraint (1-C) kinematic fit is then performed to constrain $M(\gamma\gamma)$ to the π^0 nominal mass, and the resulting 4-momentum of the candidate π^0 is used for further analysis.

We reconstruct the $D^+ \to \bar{K}^0 e^+ \nu_e$ decay by requiring exactly three additional charged tracks in the rest of the event. One track with charge opposite to that of the D^- tag is identified as a positron using the criteria mentioned above, while the other two oppositely charged tracks form a K_S^0 candidate. For the selection of the $D^+ \to \pi^0 e^+ \nu_e$ decay, we require that there is only one additional charged track consistent with the positron identification criteria and at least two photons that are used to form a π^0 candidate in the rest of the event. If there are multiple π^0 candidates, the one with the minimum χ^2 from the 1-C kinematic fit is retained. In order to additionally suppress background due to wrongly reconstructed or background photons, the semileptonic candidate is further required to have the maximum energy of any of the unused photons, $E_{\gamma,\max}$, less than 300 MeV.

Since the neutrino is undetected, the kinematic variable $U_{\text{miss}} \equiv E_{\text{miss}} - c|\vec{p}_{\text{miss}}|$ is used to obtain the information about the missing neutrino, where E_{miss} and $\vec{p}_{\text{miss}}$ are, respectively, the total missing energy and momentum in the event. The missing energy is computed from $E_{\text{miss}} = E_{\text{beam}} - E_P - E_{e^+}$, where E_P and E_{e^+} are the measured energies of the pseudoscalar meson and the positron, respectively. The missing momentum $\vec{p}_{\text{miss}}$ is given by $\vec{p}_{\text{miss}} = \vec{p}_{D^+} - \vec{p}_P - \vec{p}_{e^+}$, where $\vec{p}_{D^+}$, $\vec{p}_P$, and $\vec{p}_{e^+}$ are the 3-momenta of the D^+ meson, the pseudoscalar meson, and the positron, respectively. The 3-momentum of the D^+ meson is taken as
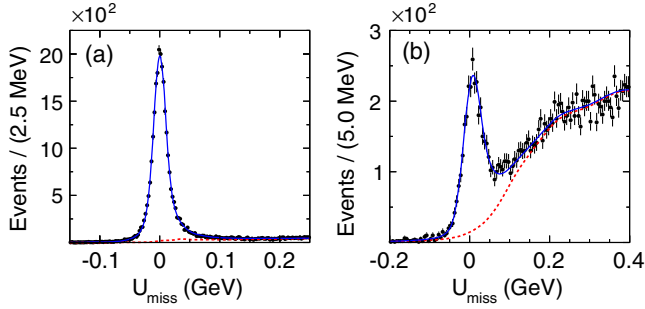
FIG. 2. Distributions of U_{miss} for the selected (a) $D^+ \rightarrow \bar{K}^0 e^+ \nu_e$ and (b) $D^+ \rightarrow \pi^0 e^+ \nu_e$ candidates (points with error bars) with fit projections overlaid (solid lines). The dashed curves show the background determined by the fit.

$\vec{p}_{D^+} = -\hat{p}_{\mathrm{tag}} \sqrt{(E_{\mathrm{beam}}/c)^2 - (m_{D^+}c)^2}$, where $\hat{p}_{\mathrm{tag}}$ is the direction of the momentum of the single D^- tag, and m_{D^+} is the D^+ mass. If the daughter particles from a semileptonic decay are correctly identified, U_{miss} is near zero, since only one neutrino is missing.

Figure 2 shows the U_{miss} distributions for the semileptonic candidates, where the potential backgrounds arise from the $D\bar{D}$ processes other than signal, $\psi(3770) \rightarrow$ non-$D\bar{D}$ decays, $e^+e^- \rightarrow \tau^+\tau^-$, continuum light hadron production, and initial state radiation return to J/ψ and $\psi(3686)$. The background for $D^+ \rightarrow \bar{K}^0 e^+ \nu_e$ is dominated by $D^+ \rightarrow \bar{K}^*(892)^0 e^+ \nu_e$ and $D^+ \rightarrow \bar{K}^0 \mu^+ \nu_\mu$. For $D^+ \rightarrow \pi^0 e^+ \nu_e$, the background is mainly from $D^+ \rightarrow K_L^0 e^+ \nu_e$ and $D^+ \rightarrow K_S^0 (\pi^0\pi^0) e^+ \nu_e$.

Following the same procedure described in Ref. [13], we perform a binned extended maximum likelihood fit to the U_{miss} distribution for each channel to separate the signal from the background component. The signal shape is
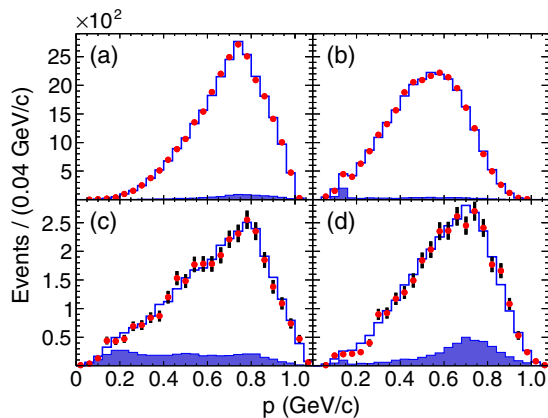

FIG. 3. Momentum distributions of selected events (with $|U_{\mathrm{miss}}| < 60$ MeV) for (a) $\bar{K}^0$, (b) e^+ from $D^+ \rightarrow \bar{K}^0 e^+ \nu_e$, (c) π^0, and (d) e^+ from $D^+ \rightarrow \pi^0 e^+ \nu_e$. The points with error bars represent data, the (blue) open histograms are MC simulated signal plus background, the shaded histograms are MC simulated background only.

constructed from a convolution of a MC determined distribution and a Gaussian function that accounts for the difference of the U_{miss} resolutions between data and MC simulation. The background shape is formed from MC simulation. From the fits shown as the overlaid curves in Fig. 2, we obtain the yields of the observed signal events to be $N_{\mathrm{obs}}(D^+ \rightarrow \bar{K}^0 e^+ \nu_e) = 26008 \pm 168$ and $N_{\mathrm{obs}}(D^+ \rightarrow \pi^0 e^+ \nu_e) = 3402 \pm 70$, respectively.

To check the quality of the MC simulation, we examine the distributions of the reconstructed kinematic variables. Figure 3 shows the comparisons of the momentum distributions of data and MC simulation.

IV. BRANCHING FRACTION MEASUREMENTS

A. Determinations of branching fractions

The branching fraction of the semileptonic decay $D^+ \rightarrow P e^+ \nu_e$ is obtained from

$$\mathcal{B}(D^+ \rightarrow P e^+ \nu_e) = \frac{N_{\mathrm{obs}}(D^+ \rightarrow P e^+ \nu_e)}{N_{\mathrm{tag}}\varepsilon(D^+ \rightarrow P e^+ \nu_e)}, \quad (2)$$

where N_{tag} is the number of D^- tags (see Sec. III A), $N_{\mathrm{obs}}(D^+ \rightarrow P e^+ \nu_e)$ is the number of observed $D^+ \rightarrow P e^+ \nu_e$ decays within the D^- tags (see Sec. III B), and $\varepsilon(D^+ \rightarrow P e^+ \nu_e)$ is the reconstruction efficiency. Here the $D^+ \rightarrow \bar{K}^0 e^+ \nu_e$ efficiency includes the K_S^0 fraction of the $\bar{K}^0$ and $K_S^0 \rightarrow \pi^+\pi^-$ branching fraction; the $D^+ \rightarrow \pi^0 e^+ \nu_e$ efficiency includes the $\pi^0 \rightarrow \gamma\gamma$ branching fraction [8].

Due to the difference in the multiplicity, the reconstruction efficiency varies slightly with the tag mode. For each tag mode i, the reconstruction efficiency is given by $\varepsilon^i = \varepsilon^i_{\mathrm{tag,SL}}/\varepsilon^i_{\mathrm{tag}}$, where the efficiency for simultaneously finding the $D^+ \rightarrow P e^+ \nu_e$ semileptonic decay and the D^- meson tagged with mode i, $\varepsilon^i_{\mathrm{tag,SL}}$ is determined using the signal MC sample, and $\varepsilon^i_{\mathrm{tag}}$ is the corresponding tag efficiency shown in Table I. These efficiencies are listed in Table II. The reconstruction efficiency for each tag mode is then weighted according to the corresponding tag yield in data to obtain the average reconstruction efficiency, $\bar{\varepsilon} = \sum_i (N^i_{\mathrm{tag}}\varepsilon^i)/N_{\mathrm{tag}}$, as listed in the last row in Table II.

Using the control samples selected from Bhabha scattering and $D\bar{D}$ events, we find that there are small discrepancies between data and MC simulation in the positron tracking efficiency, positron identification efficiency, and K_S^0 and π^0 reconstruction efficiencies. We correct for these differences by multiplying the raw efficiencies $\varepsilon(D^+ \rightarrow \bar{K}^0 e^+ \nu_e)$ and $\varepsilon(D^+ \rightarrow \pi^0 e^+ \nu_e)$ determined in MC simulation by factors of 0.9957 and 0.9910, respectively. The corrected efficiencies are found to be $\epsilon'(D^+ \rightarrow \bar{K}^0 e^+ \nu_e) = (17.75 \pm 0.03)\%$ and $\epsilon'(D^+ \rightarrow \pi^0 e^+ \nu_e) = (55.02 \pm 0.10)\%$, where the uncertainties are only statistical.

Inserting the corresponding numbers into Eq. (2) yields the absolute decay branching fractions

TABLE II.   The reconstruction efficiencies for $D^+ \to \bar{K}^0 e^+ \nu_e$ and $D^+ \to \pi^0 e^+ \nu_e$ determined from MC simulation. The efficiencies include the branching fractions for $\bar{K}^0$ and π^0. The uncertainties are statistical only.

Tag mode	$\varepsilon_{\mathrm{tag,SL}}(D^+ \to \bar{K}^0 e^+ \nu_e)$ (%)	$\varepsilon(D^+ \to \bar{K}^0 e^+ \nu_e)$ (%)	$\varepsilon_{\mathrm{tag,SL}}(D^+ \to \pi^0 e^+ \nu_e)$ (%)	$\varepsilon(D^+ \to \pi^0 e^+ \nu_e)$ (%)
$D^- \to K^+ \pi^- \pi^-$	9.21 ± 0.02	17.77 ± 0.04	28.44 ± 0.06	54.88 ± 0.13
$D^- \to K^0_S \pi^-$	10.14 ± 0.05	18.05 ± 0.11	31.15 ± 0.15	55.43 ± 0.34
$D^- \to K^0_S K^-$	9.30 ± 0.08	17.84 ± 0.22	28.68 ± 0.23	55.02 ± 0.67
$D^- \to K^+ K^- \pi^-$	7.39 ± 0.06	17.92 ± 0.18	22.53 ± 0.16	54.66 ± 0.53
$D^- \to K^+ \pi^- \pi^- \pi^0$	4.98 ± 0.02	18.25 ± 0.09	15.49 ± 0.06	56.72 ± 0.29
$D^- \to \pi^+ \pi^- \pi^-$	10.44 ± 0.11	18.34 ± 0.30	32.93 ± 0.33	57.82 ± 0.94
$D^- \to K^0_S \pi^- \pi^0$	5.67 ± 0.01	18.11 ± 0.08	17.83 ± 0.04	56.92 ± 0.25
$D^- \to K^+ \pi^- \pi^- \pi^- \pi^+$	3.50 ± 0.04	15.88 ± 0.25	11.74 ± 0.14	53.20 ± 0.81
$D^- \to K^0_S \pi^- \pi^- \pi^+$	5.55 ± 0.02	16.84 ± 0.14	18.12 ± 0.06	54.97 ± 0.45
Average		17.83 ± 0.03		55.52 ± 0.10

$$\mathcal{B}(D^+ \to \bar{K}^0 e^+ \nu_e) = (8.60 \pm 0.06 \pm 0.15) \times 10^{-2} \quad (3)$$

and

$$\mathcal{B}(D^+ \to \pi^0 e^+ \nu_e) = (3.63 \pm 0.08 \pm 0.05) \times 10^{-3}, \quad (4)$$

where the first uncertainties are statistical and the second systematic.

B. Systematic uncertainties

The systematic uncertainties in the measured branching fractions of $D^+ \to \bar{K}^0 e^+ \nu_e$ and $D^+ \to \pi^0 e^+ \nu_e$ decays include the following contributions.

Number of D^- tags. The systematic uncertainty of the number of D^- tags is 0.5% [10].

e^+ *tracking efficiency.* Using the positron samples selected from radiative Bhabha scattering events, the e^+ tracking efficiencies are measured in data and MC simulation. Considering both the polar angle and momentum distributions of the positrons in the semileptonic decays, a correction factor of 1.0021 ± 0.0019 (1.0011 ± 0.0015) is determined for the e^+ tracking efficiency in the branching fraction measurement of $D^+ \to \bar{K}^0 e^+ \nu_e$ ($D^+ \to \pi^0 e^+ \nu_e$) decay. This correction is applied and an uncertainty of 0.19% (0.15%) is used as the corresponding systematic uncertainty.

e^+ *identification efficiency.* Using the positron samples selected from radiative Bhabha scattering events, we measure the e^+ identification efficiencies in data and MC simulation. Taking both the polar angle and momentum distributions of the positrons in the semileptonic decays into account, a correction factor of 0.9993 ± 0.0016 (0.9984 ± 0.0014) is determined for the e^+ identification efficiency in the measurement of $\mathcal{B}(D^+ \to \bar{K}^0 e^+ \nu_e)$ [$\mathcal{B}(D^+ \to \pi^0 e^+ \nu_e)$]. This correction is applied, and an amount of 0.16% (0.14%) is assigned as the corresponding systematic uncertainty.

K^0_S *and π^0 reconstruction efficiency.* The momentum-dependent efficiencies for K^0_S (π^0) reconstruction in data and in MC simulation are measured with $D\bar{D}$ events. Weighting these efficiencies according to the K^0_S (π^0) momentum distribution in the semileptonic decay leads to a difference of $(-0.57 \pm 1.62)\%$ [$(-0.85 \pm 1.00)\%$] between the K^0_S (π^0) reconstruction efficiencies in data and MC simulation. Since we correct for the systematic shift, the uncertainty of the correction factor 1.62% (1.00%) is taken as the corresponding systematic uncertainty in the measured branching fraction of $D^+ \to \bar{K}^0 e^+ \nu_e$ ($D^+ \to \pi^0 e^+ \nu_e$).

Requirement on $E_{\gamma,\mathrm{max}}$. By comparing doubly tagged $D\bar{D}$ hadronic decay events in the data and MC simulation, the systematic uncertainty due to this source is estimated to be 0.1%.

Fit to the U_{miss} distribution. To estimate the uncertainties due to the fits to the U_{miss} distributions, we refit the U_{miss} distributions by varying the bin size and the tail parameters (which are used to describe the signal shapes and are determined from MC simulation) to obtain the number of signal events from D^+ semileptonic decays. We then combine the changes in the yields in quadrature to obtain the systematic uncertainty (0.12% for $D^+ \to \bar{K}^0 e^+ \nu_e$, 0.52% for $D^+ \to \pi^0 e^+ \nu_e$). Since the background function is formed from many background modes with fixed relative normalizations, we also vary the relative contributions of several of the largest background modes based on the uncertainties in their branching fractions (0.12% for $D^+ \to \bar{K}^0 e^+ \nu_e$, 0.01% for $D^+ \to \pi^0 e^+ \nu_e$). In addition, we convolute the background shapes formed from MC simulation with the same Gaussian function in the fits (0.02% for $D^+ \to \bar{K}^0 e^+ \nu_e$, 0.30% for $D^+ \to \pi^0 e^+ \nu_e$). Finally we assign the relative uncertainties to be 0.2% and 0.6% for $D^+ \to \bar{K}^0 e^+ \nu_e$ and $D^+ \to \pi^0 e^+ \nu_e$, respectively.

Form factor. In order to estimate the systematic uncertainty associated with the form factor used to generate signal events in the MC simulation, we reweight the signal

TABLE III. Summary of the systematic uncertainties considered in the measurements of the branching fractions of $D^+ \to \bar{K}^0 e^+ \nu_e$ and $D^+ \to \pi^0 e^+ \nu_e$ decays.

	Systematic uncertainty (%)	
Source	$D^+ \to \bar{K}^0 e^+ \nu_e$	$D^+ \to \pi^0 e^+ \nu_e$
Number of D^- tags	0.5	0.5
Tracking for e^+	0.19	0.15
Particle identification for e^+	0.16	0.14
K_S^0 reconstruction	1.62	$\cdots$
π^0 reconstruction	$\cdots$	1.00
Requirement on $E_{\gamma,\max}$	0.1	0.1
Fit to U_{miss} distribution	0.2	0.6
Form factor	0.2	0.2
FSR recovery	0.1	0.5
MC statistics	0.2	0.2
K_S^0/π^0 branching fraction	0.07	0.03
Total	1.76	1.41

MC events so that the q^2 spectra agree with the measured spectra. We then remeasure the branching fraction (partial decay rates in different q^2 bins) with the newly weighted efficiency (efficiency matrix). The maximum relative change of the branching fraction (partial decay rates in different q^2 bins) is 0.2% and is assigned as the systematic uncertainty.

FSR recovery. The differences between the results with FSR recovery and the ones without FSR recovery are assigned as the systematic uncertainties due to FSR recovery. We find the differences are 0.1% and 0.5% for $D^+ \to \bar{K}^0 e^+ \nu_e$ and $D^+ \to \pi^0 e^+ \nu_e$, respectively.

MC statistics. The uncertainties in the measured branching fractions due to the MC statistics are the statistical fluctuation of the MC samples, which are 0.2% for both of $D^+ \to \bar{K}^0 e^+ \nu_e$ and $D^+ \to \pi^0 e^+ \nu_e$ semileptonic decays.

K_S^0 and π^0 decay branching fractions. We include an uncertainty of 0.07% (0.03%) on the branching fraction measurement of $D^+ \to \bar{K}^0 e^+ \nu_e$ ($D^+ \to \pi^0 e^+ \nu_e$) to account for the uncertainty of the branching fraction of $K_S^0 \to \pi^+ \pi^-$ ($\pi^0 \to \gamma\gamma$) decay [8].

Table III summarizes the systematic uncertainties in the measurement of the branching fractions. Adding all systematic uncertainties in quadrature yields the total systematic uncertainties of 1.76% and 1.41% for $D^+ \to \bar{K}^0 e^+ \nu_e$ and $D^+ \to \pi^0 e^+ \nu_e$, respectively.

C. Comparison

The comparisons of our measured branching fractions for $D^+ \to \bar{K}^0 e^+ \nu_e$ and $D^+ \to \pi^0 e^+ \nu_e$ decays with those previously measured at the BES-II [14], CLEO [15], and BESIII [16,17] experiments as well as the PDG values [8] are shown in Fig. 4. Our measured branching fractions are in agreement with the other experimental measurements, but are more precise. For $D^+ \to \pi^0 e^+ \nu_e$, our result is lower than the only other existing measurement by CLEO [15] by 2.0σ.

Using our previous measurements of $\mathcal{B}(D^0 \to K^- e^+ \nu_e)$ and $\mathcal{B}(D^0 \to \pi^- e^+ \nu_e)$ [13], the results obtained in this analysis, and the lifetimes of D^0 and D^+ mesons [8], we obtain the ratios

$$I_K \equiv \frac{\Gamma(D^0 \to K^- e^+ \nu_e)}{\Gamma(D^+ \to \bar{K}^0 e^+ \nu_e)} = 1.03 \pm 0.01 \pm 0.02 \quad (5)$$

and

$$I_\pi \equiv \frac{\Gamma(D^0 \to \pi^- e^+ \nu_e)}{2\Gamma(D^+ \to \pi^0 e^+ \nu_e)} = 1.03 \pm 0.03 \pm 0.02, \quad (6)$$
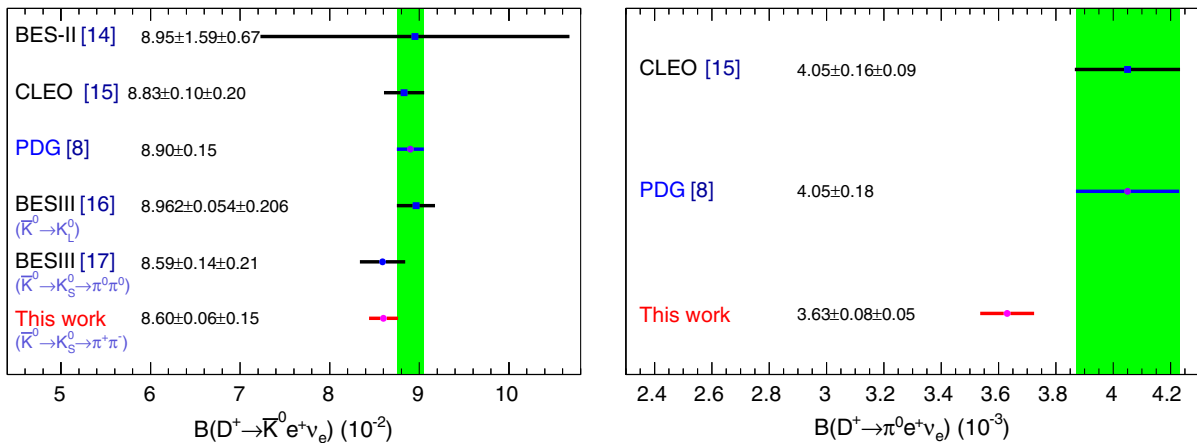
which are consistent with isospin symmetry.

FIG. 4. Comparison of the branching fraction measurements for $D^+ \to \bar{K}^0 e^+ \nu_e$ (left) and $D^+ \to \pi^0 e^+ \nu_e$ (right). The green bands correspond to the 1σ limits of the world averages.

TABLE IV. Summary of the range of each q^2 bin; the number of the observed signal events for $D^+ \to \bar{K}^0 e^+ \nu_e$ and $D^+ \to \pi^0 e^+ \nu_e$ in data.

Bin no.	1	2	3	4	5	6	7	8	9
				$D^+ \to \bar{K}^0 e^+ \nu_e$					
q^2 (GeV^2/c^4)	[0.0, 0.2)	[0.2, 0.4)	[0.4, 0.6)	[0.6, 0.8)	[0.8, 1.0)	[1.0, 1.2)	[1.2, 1.4)	[1.4, 1.6)	[1.6, $q^2_{\max}$)
$N_{\rm obs}$	5842 ± 81	4935 ± 73	4180 ± 67	3515 ± 62	2818 ± 55	2120 ± 48	1460 ± 40	860 ± 31	302 ± 19
				$D^+ \to \pi^0 e^+ \nu_e$					
q^2 (GeV^2/c^4)	[0.0, 0.3)	[0.3, 0.6)	[0.6, 0.9)	[0.9, 1.2)	[1.2, 1.5)	[1.5, 2.0)	[2.0, $q^2_{\max}$)		
$N_{\rm obs}$	658 ± 29	562 ± 27	467 ± 25	448 ± 24	401 ± 24	470 ± 26	404 ± 30		

V. PARTIAL DECAY RATE MEASUREMENTS

A. Determinations of partial decay rates

To study the differential decay rates, we divide the semileptonic candidates satisfying the selection criteria described in Sec. III into bins of q^2. Nine (seven) bins are used for $D^+ \to \bar{K}^0 e^+ \nu_e$ ($D^+ \to \pi^0 e^+ \nu_e$). The range of each bin is given in Table IV. The squared 4-momentum transfer q^2 is determined for each semileptonic candidate by $q^2 = (E_{e^+} + E_{\nu_e})^2/c^4 - (\vec{p}_{e^+} + \vec{p}_{\nu_e})^2/c^2$, where the energy and momentum of the missing neutrino are taken to be $E_{\nu_e} = E_{\rm miss}$ and $\vec{p}_{\nu_e} = E_{\rm miss}\hat{p}_{\rm miss}/c$, respectively. For each q^2 bin, we perform a maximum likelihood fit to the corresponding $U_{\rm miss}$ distribution following the same procedure described in Sec. III B and obtain the signal yields as shown in Table IV.

To account for detection efficiency and detector resolution, the number of events $N^i_{\rm obs}$ observed in the ith q^2 bin is extracted from the relation

$$N^i_{\rm obs} = \sum_{j=1}^{N_{\rm bins}} \varepsilon_{ij} N^j_{\rm prd}, \qquad (7)$$

where $N_{\rm bins}$ is the number of q^2 bins, $N^j_{\rm prd}$ is the number of semileptonic decay events produced in the tagged D^- sample with the q^2 filled in the jth bin, and ε_{ij} is the overall efficiency matrix that describes the efficiency and smearing across q^2 bins. The efficiency matrix element ε_{ij} is obtained by

$$\varepsilon_{ij} = \frac{n^{\rm rec}_{ij}}{n^{\rm gen}_j} \frac{1}{\varepsilon_{\rm tag}} f_{ij}, \qquad (8)$$

where $n^{\rm rec}_{ij}$ is the number of the signal MC events generated in the jth q^2 bin and reconstructed in the ith q^2 bin, $n^{\rm gen}_j$ is the total number of the signal MC events which are generated in the jth q^2 bin, and f_{ij} is the matrix to correct for data-MC differences in the efficiencies for e^+ tracking, e^+ identification, and $\bar{K}^0$ (π^0) reconstruction. Table V presents the

TABLE V. Efficiency matrices ε_{ij} given in percent for $D^+ \to \bar{K}^0 e^+ \nu_e$ and $D^+ \to \pi^0 e^+ \nu_e$ decays. The column gives the true q^2 bin j, while the row gives the reconstructed q^2 bin i. The statistical uncertainties in the least significant digits are given in the parentheses.

Rec. q^2	True q^2 (GeV^2/c^4)								
				$D^+ \to \bar{K}^0 e^+ \nu_e$					
(GeV^2/c^4)	[0.0, 0.2)	[0.2, 0.4)	[0.4, 0.6)	[0.6, 0.8)	[0.8, 1.0)	[1.0, 1.2)	[1.2, 1.4)	[1.4, 1.6)	[1.6, $q^2_{\max}$)
[0.0, 0.2)	18.53(6)	0.95(1)	0.07(0)	0.00(0)	0.00(0)	0.00(0)	0.00(0)	0.00(0)	0.00(0)
[0.2, 0.4)	0.37(1)	16.86(6)	1.03(2)	0.05(0)	0.00(0)	0.00(0)	0.00(0)	0.00(0)	0.00(0)
[0.4, 0.6)	0.00(0)	0.40(1)	16.03(6)	1.03(2)	0.03(0)	0.00(0)	0.00(0)	0.00(0)	0.00(0)
[0.6, 0.8)	0.00(0)	0.00(0)	0.46(1)	15.72(6)	0.95(2)	0.02(0)	0.00(0)	0.00(0)	0.00(0)
[0.8, 1.0)	0.00(0)	0.00(0)	0.01(0)	0.44(1)	15.78(7)	0.93(2)	0.01(0)	0.00(0)	0.00(0)
[1.0, 1.2)	0.00(0)	0.00(0)	0.00(0)	0.01(0)	0.46(1)	15.76(8)	0.80(2)	0.01(0)	0.00(0)
[1.2, 1.4)	0.00(0)	0.00(0)	0.00(0)	0.00(0)	0.00(0)	0.42(1)	15.58(9)	0.74(3)	0.00(0)
[1.4, 1.6)	0.00(0)	0.00(0)	0.00(0)	0.00(0)	0.00(0)	0.00(0)	0.38(2)	15.45(12)	0.78(5)
[1.6, $q^2_{\max}$)	0.00(0)	0.00(0)	0.00(0)	0.00(0)	0.00(0)	0.00(0)	0.00(0)	0.28(2)	15.98(19)
				$D^+ \to \pi^0 e^+ \nu_e$					
(GeV^2/c^4)	[0.0, 0.3)	[0.3, 0.6)	[0.6, 0.9)	[0.9, 1.2)	[1.2, 1.5)	[1.5, 2.0)	[2.0, $q^2_{\max}$)		
[0.0, 0.3)	53.84(15)	2.27(3)	0.17(1)	0.01(0)	0.00(0)	0.00(0)	0.00(0)		
[0.3, 0.6)	4.00(5)	48.24(15)	2.31(4)	0.14(1)	0.00(0)	0.00(0)	0.01(0)		
[0.6, 0.9)	0.14(1)	5.66(6)	46.15(15)	2.34(4)	0.10(1)	0.00(0)	0.00(0)		
[0.9, 1.2)	0.04(0)	0.22(1)	6.24(6)	44.51(16)	2.16(4)	0.05(0)	0.00(0)		
[1.2, 1.5)	0.04(0)	0.08(1)	0.31(1)	6.33(7)	43.33(17)	1.36(3)	0.02(0)		
[1.5, 2.0)	0.03(0)	0.08(1)	0.22(1)	0.58(2)	6.52(8)	45.48(16)	1.12(3)		
[2.0, $q^2_{\max}$)	0.13(1)	0.21(1)	0.34(1)	0.68(2)	1.30(3)	5.52(6)	50.46(19)		

average overall efficiency matrices for $D^+ \to \bar{K}^0 e^+ \nu_e$ and $D^+ \to \pi^0 e^+ \nu_e$ decays. To produce this average overall efficiency matrix, we combine the efficiency matrices for each tag mode weighted by its yield shown in Table I. The diagonal elements of the matrix give the overall efficiencies for $D^+ \to Pe^+ \nu_e$ decays to be reconstructed in the correct q^2 bins in the recoil of the single D^- tags, while the neighboring off-diagonal elements of the matrix give the overall efficiencies for cross feed between different q^2 bins.

The partial decay width in the ith bin is obtained by inverting the matrix Eq. (7),

$$\Delta\Gamma_i = \frac{N_{\mathrm{prd}}^i}{\tau_{D^+} N_{\mathrm{tag}}} = \frac{1}{\tau_{D^+} N_{\mathrm{tag}}} \sum_{j}^{N_{\mathrm{bins}}} (\varepsilon^{-1})_{ij} N_{\mathrm{obs}}^j, \qquad (9)$$

where τ_{D^+} is the lifetime of the D^+ meson [8]. The q^2-dependent partial widths for $D^+ \to \bar{K}^0 e^+ \nu_e$ and $D^+ \to \pi^0 e^+ \nu_e$ are summarized in Table VI. Also shown in Table VI are the statistical uncertainties and the associated correlation matrices.

B. Systematic covariance matrices

For each source of systematic uncertainty in the measurements of partial decay rates, we construct an

TABLE VI. Summary of the measured partial decay rates, relative statistical uncertainties, systematic uncertainties, and corresponding correlation matrices for $D^+ \to \bar{K}^0 e^+ \nu_e$ and $D^+ \to \pi^0 e^+ \nu_e$.

q^2 Bin no.	1	2	3	4	5	6	7	8	9
				$D^+ \to \bar{K}^0 e^+ \nu_e$					
$\Delta\Gamma$ (ns^{-1})	16.97	15.29	13.57	11.65	9.33	7.06	4.96	2.97	1.01
Statistical uncertainty (%)	1.45	1.61	1.75	1.91	2.12	2.44	2.92	3.77	6.56
Statistical correlation	1.000								
	−0.073	1.000							
	0.001	−0.084	1.000						
	0.000	0.003	−0.091	1.000					
	0.000	0.000	0.004	−0.085	1.000				
	0.000	0.000	0.000	0.004	−0.085	1.000			
	0.000	0.000	0.000	0.000	0.004	−0.075	1.000		
	0.000	0.000	0.000	0.000	0.000	0.004	−0.069	1.000	
	0.000	0.000	0.000	0.000	0.000	0.000	0.003	−0.059	1.000
Systematic uncertainty (%)	3.24	3.10	2.95	2.88	3.02	3.05	2.85	2.54	2.93
Systematic correlation	1.000								
	0.981	1.000							
	0.979	0.976	1.000						
	0.979	0.977	0.973	1.000					
	0.978	0.976	0.973	0.970	1.000				
	0.974	0.972	0.970	0.970	0.965	1.000			
	0.966	0.964	0.963	0.962	0.960	0.954	1.000		
	0.932	0.930	0.929	0.929	0.926	0.923	0.911	1.000	
	0.891	0.889	0.886	0.888	0.886	0.883	0.875	0.840	1.000
				$D^+ \to \pi^0 e^+ \nu_e$					
$\Delta\Gamma$ (ns^{-1})	0.664	0.578	0.474	0.477	0.432	0.503	0.372		
Statistical uncertainty (%)	4.55	5.53	6.60	6.48	7.28	6.52	8.97		
Statistical correlation	1.000								
	−0.122	1.000							
	0.011	−0.171	1.000						
	−0.002	0.019	−0.190	1.000					
	0.000	−0.003	0.021	−0.190	1.000				
	0.000	−0.001	−0.005	0.016	−0.167	1.000			
	−0.002	−0.003	−0.003	−0.008	−0.004	−0.128	1.000		
Systematic uncertainty (%)	1.53	1.52	1.51	1.61	1.88	1.92	1.73		
Systematic correlation	1.000								
	0.739	1.000							
	0.742	0.664	1.000						
	0.758	0.737	0.650	1.000					
	0.772	0.740	0.712	0.698	1.000				
	0.781	0.749	0.711	0.760	0.772	1.000			
	0.760	0.730	0.697	0.727	0.756	0.740	1.000		

$N_{\text{bins}} \times N_{\text{bins}}$ systematic covariance matrix. A brief description of each contribution follows.

D^+ lifetime. The systematic uncertainty associated with the lifetime of the D^+ meson (0.7%) [8] is fully correlated across q^2 bins.

Number of D^- tags. The systematic uncertainty from the number of the single D^- tags (0.5%) is fully correlated between q^2 bins.

e^+, K_S^0, and π^0 reconstruction. The covariance matrices for the systematic uncertainties associated with the e^+ tracking, e^+ identification, K_S^0, and π^0 reconstruction efficiencies are obtained in the following way. We first vary the corresponding correction factors according to their uncertainties, then remeasure the partial decay rates using the efficiency matrices determined from the recorrected signal MC events. The covariance matrix due to this source is assigned via $C_{ij} = \delta(\Delta\Gamma_i)\delta(\Delta\Gamma_j)$, where $\delta(\Delta\Gamma_i)$ denotes the change in the partial decay rate measurement in the ith q^2 bin.

Requirement on $E_{\gamma,\max}$. We take the systematic uncertainty of 0.1% due to the $E_{\gamma,\max}$ requirement on the selected events in each q^2 bin, and assume that this uncertainty is fully correlated between q^2 bins.

Fit to the U_{miss} distribution. The technique of fitting the U_{miss} distributions affects the number of signal events observed in the q^2 bins. The covariance matrix due to the U_{miss} fits is determined by

$$C_{ij} = \left(\frac{1}{\tau_{D^+} N_{\text{tag}}}\right)^2 \sum_\alpha \epsilon_{i\alpha}^{-1} \epsilon_{j\alpha}^{-1} [\delta(N_{\text{obs}}^\alpha)]^2, \quad (10)$$

where $\delta(N_{\text{obs}}^\alpha)$ is the systematic uncertainty of N_{obs}^α associated with the fit to the corresponding U_{miss} distribution.

Form factor. To estimate the systematic uncertainty associated with the form factor model used to generate signal events in the MC simulation, we reweight the signal MC events so that the q^2 spectra agree with the measured spectra. We then recalculate the partial decay rates in different q^2 bins with the new efficiency matrices which are determined using the weighted MC events. The covariance matrix due to this source is assigned via $C_{ij} = \delta(\Delta\Gamma_i)\delta(\Delta\Gamma_j)$, where $\delta(\Delta\Gamma_i)$ denotes the change of the partial width measurement in the ith q^2 bin.

FSR recovery. To estimate the systematic covariance matrix associated with the FSR recovery of the positron momentum, we remeasure the partial decay rates without the FSR recovery. The covariance matrix due to this source is assigned via $C_{ij} = \delta(\Delta\Gamma_i)\delta(\Delta\Gamma_j)$, where $\delta(\Delta\Gamma_i)$ denotes the change of the partial decay rate measurement in the ith q^2 bin.

MC statistics. The systematic uncertainties due to the limited size of the MC samples used to determine the efficiency matrices are translated to the covariance via

$$C_{ij} = \left(\frac{1}{\tau_{D^+} N_{\text{tag}}}\right)^2 \sum_{\alpha\beta} (N_{\text{obs}}^\alpha N_{\text{obs}}^\beta \text{cov}[\epsilon_{i\alpha}^{-1}, \epsilon_{j\beta}^{-1}]), \quad (11)$$

where the covariance of the inverse efficiency matrix elements are given by [18]

$$\text{cov}[\epsilon_{\alpha\beta}^{-1}, \epsilon_{ab}^{-1}] = \sum_{ij} (\epsilon_{\alpha i}^{-1} \epsilon_{ai}^{-1})[\sigma^2(\epsilon_{ij})]^2 (\epsilon_{j\beta}^{-1} \epsilon_{jb}^{-1}). \quad (12)$$

K_S^0 and π^0 decay branching fractions. The systematic uncertainties due to the branching fractions of $K_S^0 \to \pi^+\pi^-$ (0.07%) and $\pi^0 \to \gamma\gamma$ (0.03%) are fully correlated between q^2 bins.

The total systematic covariance matrix is obtained by summing all these matrices. Table VI summarizes the relative size of systematic uncertainties and the corresponding correlations in the measurements for the partial decay rates of the $D^+ \to \bar{K}^0 e^+ \nu_e$ and $D^+ \to \pi^0 e^+ \nu_e$ semileptonic decays.

VI. FORM FACTORS

To determine the product $f_+(0)|V_{cs(d)}|$ and other form factor parameters, we fit the measured partial decay rates using Eq. (1) with the parametrization of the form factor $f_+(q^2)$. In this analysis, we use several forms of the form factor parametrizations which are reviewed in Sec. VI A.

A. Form factor parametrizations

In general, the *single pole model* is the simplest approach to describe the q^2 dependence of the form factor. The single pole model is expressed as

$$f_+(q^2) = \frac{f_+(0)}{1 - q^2/m_{\text{pole}}^2}, \quad (13)$$

where $f_+(0)$ is the value of the form factor at $q^2 = 0$, and m_{pole} is the pole mass, which is often treated as a free parameter to improve fit quality.

The *modified pole model* [19] is also widely used in lattice QCD (LQCD) calculations and experimental studies of these decays. In this parametrization, the form factor of the semileptonic $D \to P e^+ \nu_e$ decays is written as

$$f_+(q^2) = \frac{f_+(0)}{(1 - q^2/m_{D_{(s)}^{*+}}^2)(1 - \alpha q^2/m_{D_{(s)}^{*+}}^2)}, \quad (14)$$

where $m_{D_{(s)}^{*+}}$ is the mass of the $D_{(s)}^{*+}$ meson, and α is a free parameter to be fitted.

The *ISGW2 model* [20] assumes

$$f_+(q^2) = f_+(q^2_{\max}) \left(1 + \frac{r^2}{12}(q^2_{\max} - q^2)\right)^{-2}, \quad (15)$$

where $q^2_{\max}$ is the kinematical limit of q^2, and r is the conventional radius of the meson.

The most general parametrization of the form factor is the *series expansion* [21], which is based on analyticity and unitarity. In this parametrization, the variable q^2 is mapped to a new variable z through

$$z(q^2, t_0) = \frac{\sqrt{t_+ - q^2} - \sqrt{t_+ - t_0}}{\sqrt{t_+ - q^2} + \sqrt{t_+ - t_0}}, \quad (16)$$

with $t_\pm = (m_{D^+} \pm m_P)^2$ and $t_0 = t_+(1 - \sqrt{1 - t_-/t_+})$. The form factor is then expressed in terms of the new variable z as

$$f_+(q^2) = \frac{1}{P(q^2)\phi(q^2, t_0)} \sum_{k=0}^{\infty} a_k(t_0)[z(q^2, t_0)]^k, \quad (17)$$

where $a_k(t_0)$ are real coefficients. The function $P(q^2)$ is $P(q^2) = z(t, m^2_{D^*_s})$ for $D \to K$ and $P(q^2) = 1$ for $D \to \pi$. The standard choice of $\phi(q^2, t_0)$ is

$$\phi(q^2, t_0) = \left(\frac{\pi m_c^2}{3}\right)^{1/2} \left(\frac{z(q^2, 0)}{-q^2}\right)^{5/2} \left(\frac{z(q^2, t_0)}{t_0 - q^2}\right)^{-1/2}$$
$$\times \left(\frac{z(q^2, t_-)}{t_- - q^2}\right)^{-3/4} \frac{(t_+ - q^2)}{(t_+ - t_0)^{1/4}}, \quad (18)$$

where m_c is the mass of the charm quark.

In practical use, one usually makes a truncation of the above series. After optimizing the form factor parameters, we obtain

$$f_+(q^2) = \frac{f_+(0)P(0)\phi(0, t_0)(1 + \sum_{k=1}^{k_{\max}} r_k[z(q^2, t_0)]^k)}{P(q^2)\phi(q^2, t_0)(1 + \sum_{k=1}^{k_{\max}} r_k[z(0, t_0)]^k)}, \quad (19)$$

where $r_k \equiv a_k(t_0)/a_0(t_0)$. In this analysis we fit the measured decay rates to the two- or three-parameter series expansion; i.e., we take $k_{\max} = 1$ or 2. In fact, the z expansion with only a linear term is sufficient to describe the data. Therefore we take the two-parameter series expansion as the nominal parametrization to determine $f_+^{K(\pi)}(0)$ and $|V_{cs(d)}|$.

B. Fitting partial decay rates to extract form factors

In order to determine the form factor parameters, we fit the theoretical parametrizations to the measured partial decay rates. Taking into account the correlations of the measured partial decay rates among q^2 bins, the χ^2 to be minimized in the fit is defined as

$$\chi^2 = \sum_{ij} (\Delta\Gamma_i - \Delta\Gamma_i^{\text{th}}) \mathcal{C}_{ij}^{-1} (\Delta\Gamma_j - \Delta\Gamma_j^{\text{th}}), \quad (20)$$

where $\Delta\Gamma_i$ is the measured partial decay rate in the ith q^2 bin; $\mathcal{C}_{ij}^{-1}$ is the inverse matrix of the covariance matrix $\mathcal{C}_{ij}$. In the ith q^2 bin, the theoretical expectation of the partial decay rate is obtained by integrating Eq. (1),

$$\Delta\Gamma_i^{\text{th}} = \int_{q^2_{\min,i}}^{q^2_{\max,i}} X \frac{G_F^2}{24\pi^3} |V_{cs(d)}|^2 p^3 |f_+(q^2)|^2 dq^2, \quad (21)$$

where $q^2_{\min,i}$ and $q^2_{\max,i}$ are the lower and upper boundaries of that q^2 bin, respectively.

In the fits, all parameters of the form factor parametrizations are left free. The central values of the form factor parameters are taken from the results obtained by fitting the data with the combined statistical and systematic covariance matrix together. The quadratic difference between the uncertainties of the fit parameters obtained from the fits with the combined covariance matrix and the uncertainties of the fit parameters obtained from the fits with the statistical covariance matrix only is taken as the systematic error of the measured form factor parameter. The results of these fits are summarized in Table VII, where the first errors are statistical and the second systematic.

Figure 5 shows the fits to the measured differential decay rates for $D^+ \to \bar{K}^0 e^+ \nu_e$ and $D^+ \to \pi^0 e^+ \nu_e$. Figure 6 shows the projection of the fits onto $f_+(q^2)$ for the $D^+ \to \bar{K}^0 e^+ \nu_e$ and $D^+ \to \pi^0 e^+ \nu_e$ decays, respectively. In these two figures, the dots with error bars show the measured values of the form factors, $f_+(q^2)$, in the center of each q^2 bin, which are obtained with

$$f_+(q_i^2) = \sqrt{\frac{\Delta\Gamma_i}{\Delta q_i^2} \frac{24\pi^3}{X G_F^2 p_i'^3 |V_{cq}|^2}} \quad (22)$$

in which

$$p_i'^3 = \frac{\int_{q^2_{\min,i}}^{q^2_{\max,i}} p^3 |f_+(q^2)|^2 dq^2}{|f_+(q_i^2)|^2 (q^2_{\max,i} - q^2_{\min,i})}, \quad (23)$$

TABLE VII.   Summary of results of form factor fits for $D^+ \to \bar{K}^0 e^+ \nu_e$ and $D^+ \to \pi^0 e^+ \nu_e$, where the first errors are statistical and the second systematic.

Single pole model		
Decay mode	$f_+(0)|V_{cq}|$	m_{pole} (GeeV/c^2)
$D^+ \to \bar{K}^0 e^+ \nu_e$	$0.7094 \pm 0.0035 \pm 0.0111$	$1.935 \pm 0.017 \pm 0.006$
$D^+ \to \pi^0 e^+ \nu_e$	$0.1429 \pm 0.0020 \pm 0.0009$	$1.898 \pm 0.020 \pm 0.003$
Modified pole model		
Decay mode	$f_+(0)|V_{cq}|$	α
$D^+ \to \bar{K}^0 e^+ \nu_e$	$0.7052 \pm 0.0038 \pm 0.0112$	$0.294 \pm 0.031 \pm 0.010$
$D^+ \to \pi^0 e^+ \nu_e$	$0.1400 \pm 0.0024 \pm 0.0010$	$0.285 \pm 0.057 \pm 0.010$
ISGW2 model		
Decay mode	$f_+(0)|V_{cq}|$	r (GeV$^{-1}c^2$)
$D^+ \to \bar{K}^0 e^+ \nu_e$	$0.7039 \pm 0.0037 \pm 0.0111$	$1.587 \pm 0.023 \pm 0.007$
$D^+ \to \pi^0 e^+ \nu_e$	$0.1381 \pm 0.0023 \pm 0.0007$	$2.078 \pm 0.067 \pm 0.011$
Two-parameter series expansion		
Decay mode	$f_+(0)|V_{cq}|$	r_1
$D^+ \to \bar{K}^0 e^+ \nu_e$	$0.7053 \pm 0.0040 \pm 0.0112$	$-2.18 \pm 0.14 \pm 0.05$
$D^+ \to \pi^0 e^+ \nu_e$	$0.1400 \pm 0.0026 \pm 0.0007$	$-2.01 \pm 0.13 \pm 0.02$

Three-parameter series expansion			
Decay mode	$f_+(0)|V_{cq}|$	r_1	r_2
$D^+ \to \bar{K}^0 e^+ \nu_e$	$0.6983 \pm 0.0056 \pm 0.0112$	$-1.76 \pm 0.25 \pm 0.06$	$-13.4 \pm 6.3 \pm 1.4$
$D^+ \to \pi^0 e^+ \nu_e$	$0.1413 \pm 0.0035 \pm 0.0012$	$-2.23 \pm 0.42 \pm 0.06$	$1.4 \pm 2.5 \pm 0.4$

where $|V_{cs}| = 0.97351 \pm 0.00013$ and $|V_{cd}| = 0.22492 \pm 0.00050$ are taken from the SM constraint fit [8]. In the calculation of $p_i'^3$, $f_+(q^2)$ is computed using the two-parameter series parametrization with the measured parameters.

C. Determinations of $f_+^K(0)$ and $f_+^\pi(0)$

Using the $f_+^{K(\pi)}(0)|V_{cs(d)}|$ values from the two-parameter series expansion fits and taking the values of $|V_{cs(d)}|$ from the SM constraint fit [8] as inputs, we obtain the form factors
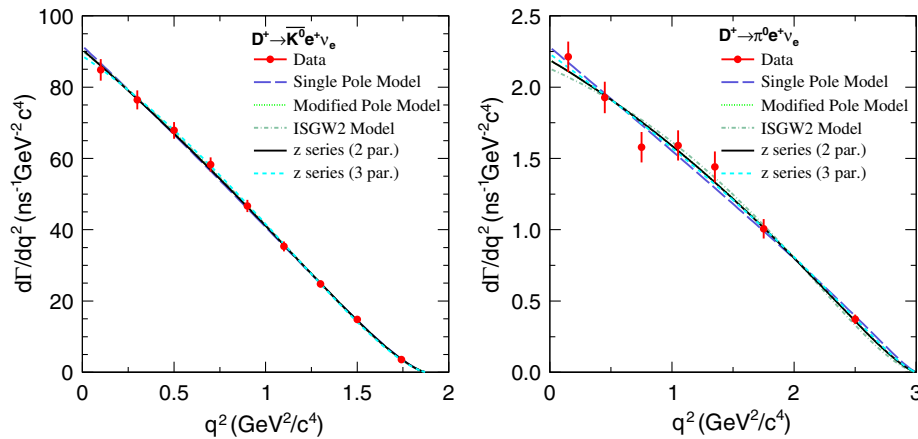

FIG. 5.   Differential decay rates for $D^+ \to \bar{K}^0 e^+ \nu_e$ (left) and $D^+ \to \pi^0 e^+ \nu_e$ (right) as a function of q^2. The dots with error bars show the data and the lines give the best fits to the data with different form factor parametrizations.
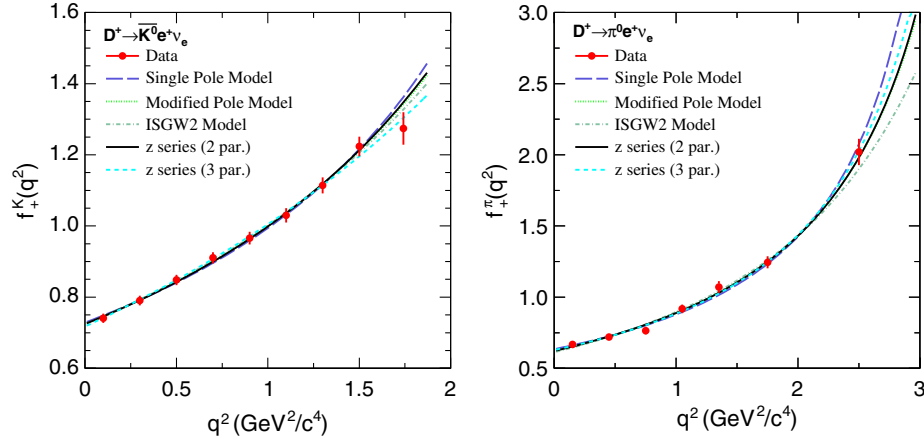
FIG. 6.   Projections on $f_+(q^2)$ for $D^+ \to \bar{K}^0 e^+ \nu_e$ (left) and $D^+ \to \pi^0 e^+ \nu_e$ (right) as a function of q^2, where the dots with error bars show the data and the lines give the best fits to the data with different form factor parametrizations.

$$f_+^K(0) = 0.725 \pm 0.004 \pm 0.012 \qquad (24)$$

and

$$f_+^\pi(0) = 0.622 \pm 0.012 \pm 0.003, \qquad (25)$$

where the first errors are statistical and the second systematic.

VII. DETERMINATIONS OF $|V_{cs}|$ AND $|V_{cd}|$

Using the values of $f_+^{K(\pi)}(0)|V_{cs(d)}|$ from the two-parameter z-series expansion fits and in conjunction with the form factor values $f_+^K(0) = 0.747 \pm 0.011 \pm 0.015$ [22] and $f_+^\pi(0) = 0.666 \pm 0.020 \pm 0.021$ [23] calculated from LQCD, we obtain

$$|V_{cs}| = 0.944 \pm 0.005 \pm 0.015 \pm 0.024 \qquad (26)$$

and

$$|V_{cd}| = 0.210 \pm 0.004 \pm 0.001 \pm 0.009, \qquad (27)$$

where the first uncertainties are statistical, the second systematic, and the third are due to the theoretical uncertainties in the LQCD calculations of the form factors.

VIII. SUMMARY

In summary, by analyzing 2.93 fb^{-1} of data collected at 3.773 GeV with the BESIII detector at the BEPCII, the semileptonic decays for $D^+ \to \bar{K}^0 e^+ \nu_e$ and $D^+ \to \pi^0 e^+ \nu_e$ have been studied. From a total of 1703054 ± 3405 D^- tags, 26008 ± 168 $D^+ \to \bar{K}^0 e^+ \nu_e$ and 3402 ± 70 $D^+ \to \pi^0 e^+ \nu_e$ signal events are observed in the system recoiling against the D^- tags. These yield the absolute decay branching fractions to be $\mathcal{B}(D^+ \to \bar{K}^0 e^+ \nu_e) = (8.60 \pm 0.06 \pm 0.15) \times 10^{-2}$ and $\mathcal{B}(D^+ \to \pi^0 e^+ \nu_e) = (3.63 \pm 0.08 \pm 0.05) \times 10^{-3}$.

We have also studied the relations between the partial decay rates and squared 4-momentum transfer q^2 for these two decays and obtained the parameters of different form factor parametrizations. The products of the form factors and the related CKM matrix elements extracted from the two-parameter series expansion parametrization have been selected as our primary results. We have obtained $f_+(0)|V_{cs}| = 0.7053 \pm 0.0040 \pm 0.0112$ and $f_+(0)|V_{cd}| = 0.1400 \pm 0.0026 \pm 0.0007$. Using the global SM fit values for $|V_{cs}|$ and $|V_{cd}|$, we have obtained the form factors $f_+^K(0) = 0.725 \pm 0.004 \pm 0.012$ and $f_+^\pi(0) = 0.622 \pm 0.012 \pm 0.003$. Furthermore, using the form factors predicted by the LQCD calculations, we have obtained the CKM matrix elements $|V_{cs}| = 0.944 \pm 0.005 \pm 0.015 \pm 0.024$ and $|V_{cd}| = 0.210 \pm 0.004 \pm 0.001 \pm 0.009$, where the third errors are dominated by the theoretical uncertainties in the LQCD calculations of the form factors.

[1] J. G. Köerner and G. A. Schuler, Z. Phys. C **46**, 93 (1990); F. J. Gilman and R. L. Singleton, Jr., Phys. Rev. D **41**, 142 (1990).

[2] M. Ablikim *et al.* (BESIII Collaboration), Chin. Phys. C **37**, 123001 (2013); Phys. Lett. B **753**, 629 (2016).

[3] M. Ablikim *et al.* (BESIII Collaboration), Nucl. Instrum. Methods Phys. Res., Sect. A **614**, 345 (2010).

[4] S. Agostinelli *et al.* (GEANT4 Collaboration), Nucl. Instrum. Methods Phys. Res., Sect. A **506**, 250 (2003).

[5] Z. Y. Deng *et al.*, Chin. Phys. C **30**, 371 (2006).

[6] S. Jadach, B. F. L. Ward, and Z. Was, Comput. Phys. Commun. **130**, 260 (2000).

[7] D. J. Lange, Nucl. Instrum. Methods Phys. Res., Sect. A **462**, 152 (2001); R.-G. Ping, Chin. Phys. C **32**, 599 (2008).

[8] C. Patrignani *et al.* (Particle Data Group Collaboration), Chin. Phys. C **40**, 100001 (2016).

[9] J. C. Chen, G. S. Huang, X. R. Qi, D. H. Zhang, and Y. S. Zhu, Phys. Rev. D **62**, 034003 (2000).

[10] M. Ablikim *et al.* (BESIII Collaboration), Phys. Rev. D **89**, 051104(R) (2014).

[11] H. Albrecht *et al.* (ARGUS Collaboration), Phys. Lett. B **241**, 278 (1990).

[12] M. Ablikim *et al.* (BES Collaboration), Phys. Lett. B **597**, 39 (2004).

[13] M. Ablikim *et al.* (BESIII Collaboration), Phys. Rev. D **92**, 072012 (2015).

[14] M. Ablikim *et al.* (BES Collaboration), Phys. Lett. B **608**, 24 (2005).

[15] D. Besson *et al.* (CLEO Collaboration), Phys. Rev. D **80**, 032005 (2009).

[16] M. Ablikim *et al.* (BESIII Collaboration), Phys. Rev. D **92**, 112008 (2015).

[17] M. Ablikim *et al.* (BESIII Collaboration), Chin. Phys. C **40**, 113001 (2016).

[18] M. Lefebvre, R. K. Keeler, R. Sobie, and J. White, Nucl. Instrum. Methods Phys. Res., Sect. A **451**, 520 (2000).

[19] D. Becirevcic and A. B. Kaidalov, Phys. Lett. B **478**, 417 (2000).

[20] D. Scora and N. Isgur, Phys. Rev. D **52**, 2783 (1995).

[21] T. Becher and R. J. Hill, Phys. Lett. B **633**, 61 (2006).

[22] H. Na, C. T. H. Davies, E. Follana, G. P. Lepage, and J. Shigemitsu, Phys. Rev. D **82**, 114506 (2010).

[23] H. Na, C. T. H. Davies, E. Follana, J. Koponen, G. P. Lepage, and J. Shigemitsu, Phys. Rev. D **84**, 114505 (2011).